

# Site investigation and characterization of the slope stability at the Drachenfels, Germany

Dominik Johann

*Stölben GmbH, Zell (Mosel), Germany, d.johann@stoelben-gmbh.de*

Volker Eitner

*Geopartner S.à r.l., Niederanven, Luxembourg, volker.eitner@geopartner.lu*

Ferdinand Stölben

*Geopartner GmbH, Zell (Mosel), Germany, ferdinand.stoelben@geopartner.biz*

Roland Strauss

*Geologischer Dienst Nordrhein-Westfalen, Krefeld, Germany, roland.strauss@gd.nrw.de*

**ABSTRACT:** The Drachenfels is located at the Rhine River opposite of the city of Bonn. It is formed by trachyte. The slopes of the Drachenfels are very steep and instable due to the former use as a quarry. The slopes were stabilized in the past but due to aging the stabilization of the rock was endangered. The structure of joints was therefore analyzed by using the scanline technique in order to examine the possibility of slope failures. Manual, laser and televue measurements were also used to evaluate the structure. The rock mechanical and physical properties of the trachyte were determined by laboratory tests. The subsequent stabilization of unstable parts of the slope has been realized by the application of software models and calculations. Based on the gained data, a risk assessment of possible rock falls was finally made. The evaluation of the data revealed seven main orientations of joints in the slope. Laboratory tests showed the low uniaxial compressive strength, the roughness of the joint surfaces and the high susceptibility of frost as some of the most concise properties of the trachyte. As a result, it can be shown that blocks and slide wedges are formed by the intersection of these joints which can slide and tip due to a low safety factor. These loose, blocky rocks, rock spurs, overhangs and unstable rock formations could only be secured by an exchange of aged tendons and additional anchors, nails and rope nets made from high-tensile wire. The monitoring of the rock will be continued by geodetic and geotechnical measurements like pressure cells at the anchors and tendons.

**Keywords:** slope stabilization, trachyte, rockfall, risk assessment

## 1. Introduction

The Drachenfels (means dragon's rock in English) is located at the Rhine River opposite of the city of Bonn. The rock is formed by the remnants of a volcano and has been the site of a trachyte quarry since Roman times, which, amongst others, delivered the building material for the Cologne Cathedral. The rock itself and the ruins on top of the Drachenfels gained popularity in the romantic era, after the Napoleonic Wars had ended. The visit of Lord Byron to the Rhine Valley and its appearance in his poem "Childe Harold's Pilgrimage" provided the rock with international attention. It soon became a highlight of the so-called Rhine romanticism and is still a touristic hotspot with a lot of visitors.

The slopes of the Drachenfels are very steep and instable due to the former use as a quarry. They were stabilized in the past; the latest and most extensive stabilization was carried out in the early 1970s by using anchors, tendons, nails and shotcrete. The aging of the anchors and tendons was monitored since the beginning. Some of the anchors and tendons showed a decreasing tensile strength. Moreover, recent rock falls endangered the safe use of a popular pathway to the top of the rock.

First, a north-south trending 60 m high, almost vertical slope was investigated and stabilized. Therefore, a scaffolding was erected for the entire height of this slope

which allowed a direct access to the rock without mountaineering skills.

The stability of slopes depends on many different parameters. Important internal factors include the slope inclination, the slope geometry, the mechanical behavior, the tectonic structure and the seepage along the joints. External factors such as precipitation, effects of frost, load changes, tectonic loosening or seismic influence can lead to changes in the individual parameters. These changes can endanger the stability of a slope. The mechanical behavior of the rock and the influence of frost were investigated experimentally in this work as these are the main factors for the Drachenfels. The tectonic structure of the slope was recorded by means of manual measurements. Moreover, the typical failure mechanisms of rock slopes like planar failure, wedge failure and toppling were analyzed.

### 1.1. Site location

The Drachenfels is located southeast of the city of Bonn, Germany in the Rhine valley, (see Figure 1). It is an approximately 900 km<sup>2</sup> volcanic area of the Siebengebirge mountains.

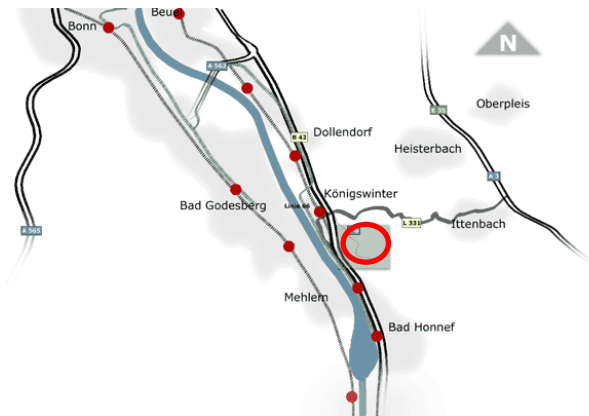


Figure 1. Location of the Drachenfels (Source: www.drachenfels.net)

## 1.2. Geology

The Drachenfels was formed about 25 million years ago in the Oligocene by the rise of a trachytic magma. The rising magma did not break through the surface but solidified in the previously deposited tuffs and formed a trachytic cryptodome. This volcanic structure was later exposed by erosion of the river Rhine. The trachyte contains several centimeter-sized sanidine crystals. The tabular sanidines which had previously crystallized in a deeper magma chamber were thereby regulated into the dome-shaped flow structure.

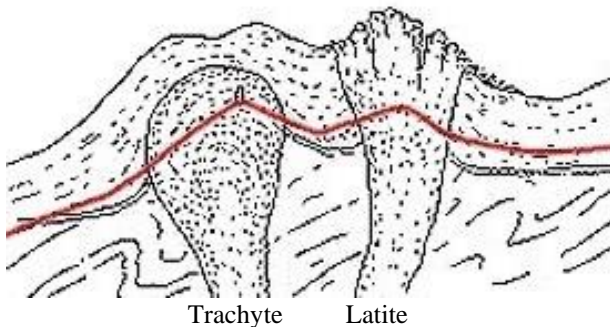


Figure 2. Cryptodome of Drachenfels (from Wunderlich 1968, modified)

## 1.3. Tectonics

Four main joint systems can be identified at the Drachenfels:

Strike	Dip angle	Dip direction
NE – SW	50° to 90°	NW and SE
E – W	50° to 90°	N and S
SE – NW	60° to 90°	SW and NE
N – S	60° to 90°	W, partly E

The NE-SW and SE-NW striking major joints are predominant. The spacing is about 2 m to 3 m. The extension ranges between a few meters and more than 30 m. The extent and the distance of the minor joints are only a few decimeters to a few meters.

The joint spacing varies between a few millimeters and a few centimeters; but they can also be up to half a meter.

Intersecting lines of joints have created wedge-shaped rock outcrops. The joints and the weathering create perpendicular boulders which will loosen and fall down sooner or later.

The open joints sometimes reach far inside the rock mass, through which rainwater can penetrate the mountain. In winter, this can lead to frost weathering.

## 1.4. Trachyte

The trachyte is characterized by a fine-grained dense groundmass formed by plagioclase, augite, apatite and biotite. A peculiarity of the Drachenfels trachytes is the centimeter-sized Sanidine inclusions, which thus forms a specific mineral of the trachyte.

The Drachenfels trachyte exhibits an extreme heterogeneity due to the different sizes and distributions of the sanidine.

Accessorily, orthoclase, titanite and partially zirconium occur. The light color of the matrix is formed by the plagioclase and the apatites.

A characteristic of the rock is the roughness of fracture surfaces and edges.

## 2. Investigation methods

### 2.1. Analysis of the discontinuities

The discontinuities were analyzed by using manual measurements, laser scanning and televue data during the field work campaign.

#### 2.1.1. Manual measurements

The recording of the discontinuities and their properties was carried out using the scanline method according to [2]. In this method, a tape measure is stretched horizontally or vertically along the slope.

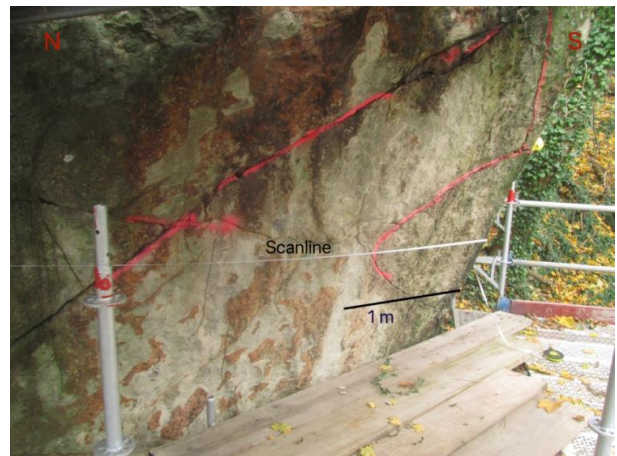


Figure 3. Scanline with a length of 4,28 m at the slope

First, the orientation of the scanline is measured with a geological compass. Then, all discontinuities that cross the tape measure are measured including joints, stratifications, faults etc. The orientation and the type of discontinuity are determined. In addition, their opening width, the spacing and the length are measured. For this purpose, the roughness, the waviness and the progression of

the discontinuities are evaluated. A distinction is made between discontinuities that end up in intact rock and those ending in another discontinuity. An initial assessment of the compressive strength and the degree of weathering of the joint can be made by a pressure test hammer (Schmidt hammer).

The aim of the scanline method is to calculate the true spacing of the joints. The spacing and the orientations were calculated by the program Dips 7.0 [6]. The evaluation of the measured structural data enabled an analysis of the failure possibilities of the slope. The spacing is also needed in the analysis of the failure mechanisms.

### 2.1.2. Laser scanning

In April 2017, the Geological Survey (GD NRW) carried out a laser scan of the Drachenfels dome (see and analysis of the discontinuities).

The examination and evaluation of discontinuities such as joints can be carried out using modern three-dimensional methods such as laser scanning or digital photogrammetry, also known as light detection and ranging (LIDAR).

The slope was recorded three-dimensionally using a terrestrial laser scanner (Faro Focus3DX\_330). The acquired digital data was processed with the software FaroScene [10] to a three-dimensional point cloud.

In a further step, normals were calculated for each point of the point cloud (with a Hough transformation) and converted into incident and incidence values accordingly. The visualization and processing of the point cloud data is done using CloudCompare [9], an open-source point cloud processing software.

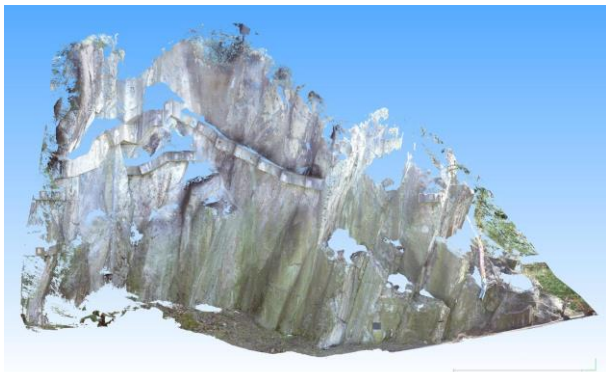


**Figure 4.** North-south striking slope of the Drachenfels

A point cloud reduced to an average point distance of about 1,5 cm was then classified and analyzed with respect to the orientation of discontinuities. For this purpose, a method according to [4] and the open-source software "Discontinuity Set Extractor" from [3] were used. The parameters of the discontinuities such as direction/dip, area ratio, spacing and standard deviation were also determined with this software.

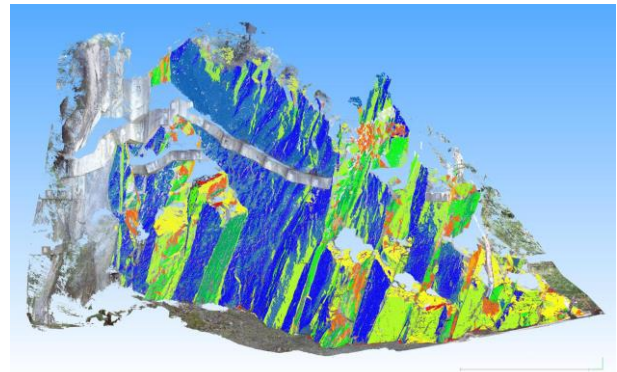


**Figure 5.** Point cloud captured with terrestrial laser scanner, colored with RGB values from digital photos

The parameter discontinuity extension refers to the total cumulative length of the discontinuities of a given discontinuity direction and is a rough estimate derived from the geometries of the surfaces.

## 2.2. Rock mechanical characterization

### 2.2.1. Rock mechanical testing

For the analysis of the slope stability, the rock mechanical properties of the trachyte were characterized. Its dry density, bulk density, grain density, porosity and void ratio were determined by laboratory tests. The strength properties of the weathered and unweathered trachyte were determined by uniaxial and triaxial tests, Brazilian tests, direct shear tests and slake durability tests.

### 2.2.2. Ultrasonic measurements

Further knowledge about the rock properties was provided by ultrasonic measurements and permeability tests. In order to investigate the influence of temperature fluctuations on the rock, a freeze-thaw cycle was performed on the samples.

Ultrasonic measurement is a method for determining the dynamic elastic properties of a rock by the transmission speed of elastic waves. These are divided into compression waves (primary waves)  $V_p$  [km / s] and shear waves (secondary waves)  $V_s$  [km / s]. The primary waves are characterized by longitudinal vibrations parallel to the propagation direction. In secondary waves, transverse vibrations occur perpendicular to the propagation direction. The velocity of  $V_p$  waves in rocks depends mainly on the density, the water content and the degree of weathering of the material (Gillhuber, 2010). The change in the texture of a rock can be studied by measuring the wave velocity. The influence of frost can destroy the structure of the rock, which can influence the stability of the slope. This process would be apparent by the decrease in shaft speed. For this reason, the samples treated by frost and thaw were examined for their degree of weathering by means of ultrasonic measurements. In addition, ultrasonic measurements were carried out with untreated samples in saturated and unsaturated state.

The test preparation consists of stretching the cylindrical sample (length approx. 80 mm and diameter

approx. 40 mm) horizontally between a pulse generator and a receiver. With the help of air pressure (with all samples approx. 800 hPa) the sample is held and is lying freely in the air.

Using a generator (Geotron USG-40), an elastic wave is transmitted in the longitudinal direction through the sample via the pulse generator. The generator is set to a frequency of 20 kHz. A receiver (Geotron UPE-D) converts the vibration into an electrical signal picked up by a transducer (Geotron UPE-G). The evaluation of the data is carried out with the help of the program Dehnwelle. The length, diameter and weight of the sample are entered into the program before the measurement. The  $V_p$  velocity is calculated from the quotient of the sample length  $l$  [mm] and the transit time  $t$  [s] required by the pulse to pass through the sample.

### 2.2.3. Frost-thaw cycle

A consequence of the physical weathering is the mechanical disintegration of rock by a loosening of the structure or the destruction of individual grains. Important processes in physical weathering are thermal and frost weathering. Large temperature fluctuations can lead to expansion of the minerals and thus weakening of the rock structure. For the consideration of the slope stability, the influence of frost is an important factor. Therefore, the possible effect of frost on the Drachenfels trachyte had to be checked.

By a possible loosening and destruction of the structure, the cohesion of the rock can be reduced. In addition, the effect of water in conjunction with frost can significantly affect the discontinuity properties. For these reasons, a decrease in the holding forces and thus a reduction of the slope stability would occur. Therefore, frost-thaw tests were carried out.

Frost weathering is caused by the infiltration of water into the rock mass. The freezing of water leads to an increase in volume, from which fissures, material detachment and a decrease in density may result. Therefore, the frost-thaw cycle was performed on unweathered and weathered trachyte specimens. The test was carried out in a slightly modified way as specified in [1].

Two unweathered and two weathered cylindrical samples were used for the test. After measuring the length and diameter of the samples, the samples are saturated with distilled water using a desiccator. Subsequently, the saturated samples are placed in a container filled with distilled water and stored in a refrigerator at  $-19,9^\circ\text{C}$  for at least 48 hours. After this freezing period, the samples are thawed for about 2 hours and then weighed and measured. After this first frost-thaw cycle, the samples are stored again in the refrigerator. The test series consisted of 13 freeze-thaw cycles.

Ultrasonic measurements are made to analyse possible changes in the samples. The respective  $V_p$  speed is measured. To determine any possible change in rock properties, ultrasonic measurements are made on the dry and saturated samples and after each cycle.

## 3. Investigation results

### 3.1. Results of laboratory testing

According to the laboratory tests the trachyte has the following rock mechanical properties:

- Dry density: approx.  $2,25\text{ g/cm}^3$
- bulk density: approx.  $22\text{ N/m}^3$
- grain density: approx.  $2,65\text{ g/cm}^3$
- porosity: approx 15%
- void ratio: approx. 0,16

The physical changes of the samples during the freeze-thaw test were documented by the measurement of  $V_p$  waves. The following Table 1 lists the  $V_p$  velocities of the four samples tested during the frost-thaw cycle.

**Table 1.**  $V_p$  velocity in the course of a frost-thaw cycle

Frost-thaw cycle	V1,1	V1,2	UV1,1	UV1,2
	$V_p$ velocity (km/s)			
dry	2,702	2,436	3,008	2,923
saturated	3,090	2,465	3,699	2,965
1	3,092	2,459	3,611	2,934
2	3,150	2,524	3,584	3,057
3	3,026	2,473	3,365	2,928
4	2,973	2,353	2,976	2,770
5	2,584	2,322	2,861	2,772
6	2,584	2,278	2,781	2,566
7	3,051	2,316	2,747	2,367
8	2,599	2,272	2,790	2,161
9	2,303	2,148	2,594	2,291
10	2,494	2,027	2,409	2,252
11	2,451	2,117	2,573	2,176
12	2,437	2,143	2,392	2,143
13	2,479	2,31	2,235	1,986
Dry after frost-thaw cycle	1,987	1,977	1,563	1,441

The decrease in the shaft speeds is shown graphically in Figure 6.

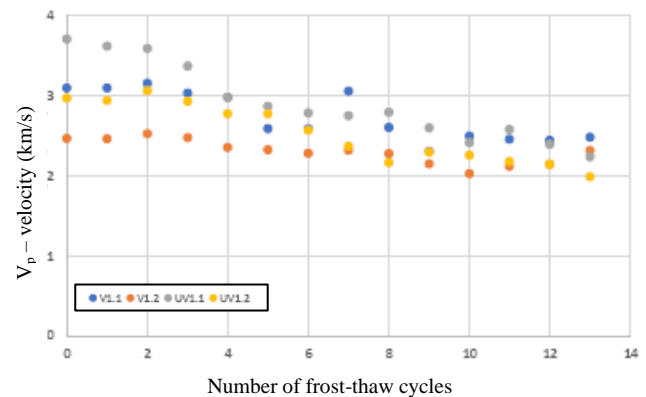


**Figure 6.**  $V_p$  velocities during the frost-thaw cycle

In addition to the measurement of  $V_p$  velocities, the macroscopic changes of the samples during the frost-thaw cycle were examined. Significant material abrasion and crack formation can be seen especially in the unweathered samples UV 1,1 and UV 1,2 (see Figure 7)



**Figure 7.** Unweathered Samples UV 1,1 and UV 1,2 after the 10<sup>th</sup> frost-thaw cycle

Both the fine matrix and the larger sanidine crystals show material disintegration. After the third frost-thaw cycle, a first abrasion can be seen on the unweathered samples. After the sixth frost-thaw period, the weathered samples also show a first loss of material. Significant crack formations can be seen on sample UV 1,1 after the tenth cycle, whereas sample UV 1,2 has only cracked. The formation of cracks can also be seen microscopically in a thin section of sample UV 1,1 (see Figure 8).

The first two photos of Figure 8 show a roughly 0,2 mm wide crack (dyed blue), which runs along a sanitary single crystal.

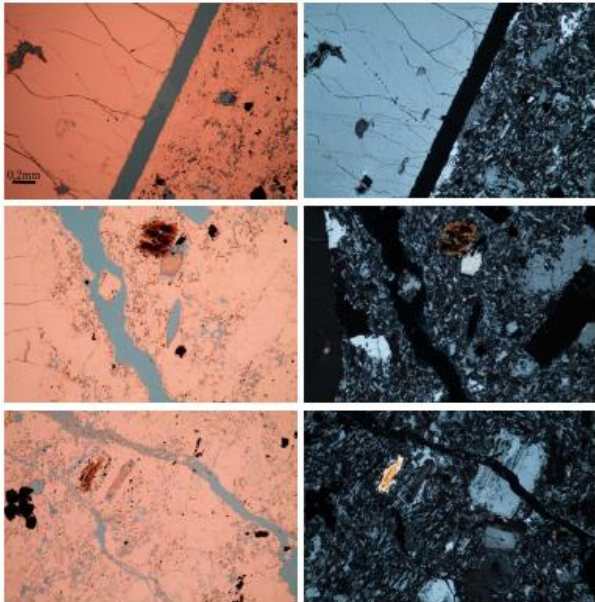


**Figure 8.** Thin section of sample UV 1,1

The picture shows only a section of the sanidine, but the crack runs around the entire crystal. From there, a further course of the crack can be recognized by the fine matrix (consisting of sanidine and plagioclase) of the sample. This further course of the crack can be seen in the two images below. In the last two thin sections, it can be seen that an approximately 0,1 mm wide crack has

formed, which runs through the fine matrix of the rock and an approximately 0,5 mm plagioclase.

The loss of material of the individual samples can also be recognized by measuring the weight.

In addition to the weight losses, in the course of the frost-thaw cycle, length and diameter expansions are shown, which are shown in Table 2.

**Table 2.** Extension of length and diameter of the samples in a course of a frost-thaw cycle

Sample	Length Start [mm]	Length End [mm]	Diameter Start [mm]	Diameter End [mm]
V1,1	84,20	84,38	39,78	39,80
V1,2	85,63	85,74	39,79	39,79
UV 1,1	87,09	87,60	39,79	40,01
UV 1,2	81,78	82,27	39,75	39,93

The uniaxial compressive strength values are clearly different in both the weathered and the unweathered samples. The highest uniaxial compressive strength of the unweathered rock varies between 41 MPa and 57 MPa.

The weathered samples have an uniaxial compressive strengths between 30 MPa and 47 MPa.

Despite a previous frost-thaw cycle, the weathered samples have higher compressive strengths of 48 MPa and 51 MPa, respectively.

The values of the moduli of elasticity are in a range of 6,38 GPa and 11,23 GPa . The values of the deformation moduli show a difference between the untreated (9,63 GPa) and the freeze-thawed samples (4,54 GPa and 5,59 GPa)

The Poisson's values of the untreated rock samples vary between 0,21 and 0,26 and those of the samples treated by freeze-thaw tests between 0,22 and 0,25.

For the 60 meter high nearly vertical slope of the Drachenfels the ground stress is 1,3 MPa with a density of 2200 kg / m<sup>3</sup>.

The tensile strength of four samples were determined by Brazilian Tests. They range from 4824 N to 6804 N.

The results of the triaxial test can be used to determine the failure criteria according to Mohr-Coulomb and Hoek-Brown for the weathered and unweathered trachyte specimens. In addition, the results of uniaxial compressive strengths and tensile strengths were used to determine the failure criterion. These are shown in the Figures 9 and 10.

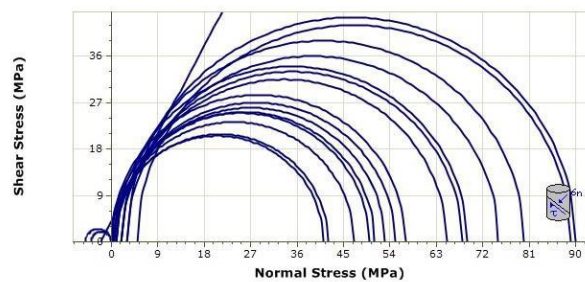


**Figure 9.** Failure criterion according to Mohr-Coulomb for the unweathered trachyte samples

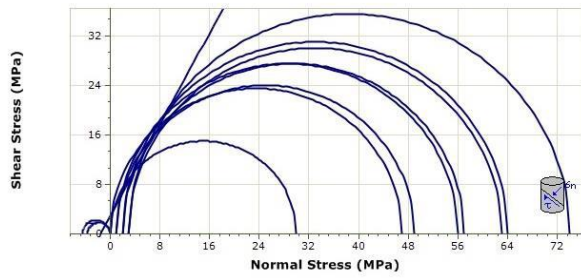


Figure 10. Failure criterion according to Mohr-Coulomb for the weathered trachyte samples

The stresses determined from the triaxial and uniaxial compression tests and the tensile tests are plotted in a  $\sigma_1$ - $\sigma_3$  graph. In Figure 11 a) the tensions of the unweathered samples and in Figure 11 b) the tensions of the weathered samples are plotted.

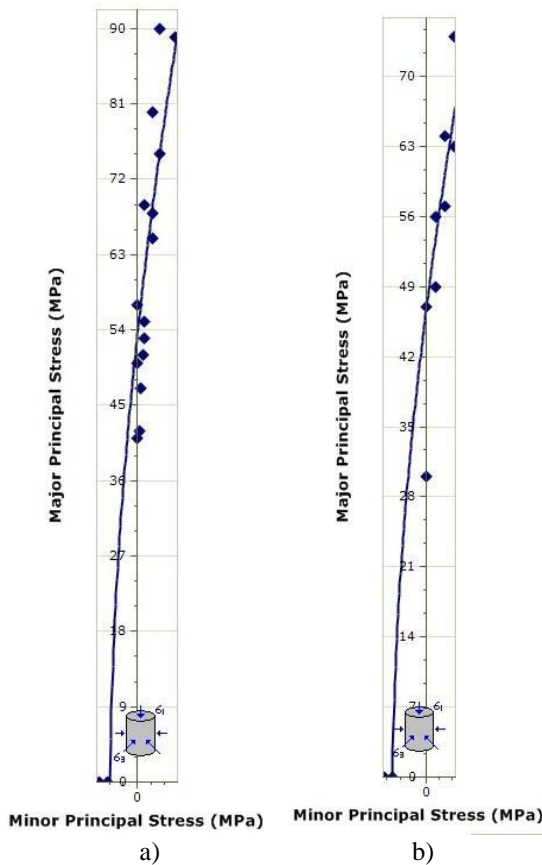


Figure 11. Failure criterion after Hoek-Brown

By forming the failure criterion according to Hoek-Brown, the intact uniaxial compressive strength of the rock and the material constant  $m_i$  are calculated with the help of the software RocData 5.0. The determination of the internal friction angle and the cohesion of the samples is carried out by the formation of the breakage criterion according to Mohr-Coulomb.

The intact uniaxial compressive strengths are 53,2 MPa for the unweathered trachyte and 46,5 MPa for the weathered material.

The values of the material constant  $m_i$  also show a clear difference. The  $m_i$  value of the weathered trachyte is 15,1, while the weathered value is 12,8. The internal friction angles are close to each other with values of  $62,1^\circ$  (unweathered) and  $61,5^\circ$  (weathered). The cohesion of

the unweathered trachyte is 4,01 MPa and the weathered 2,96 MPa.

For the calculation of the rock strength  $\sigma_{1s}$  first the RMR value and the constant  $s$  had to be determined. The addition of the RQD index (20), the discontinuity spacing (15), the state of the discontinuities (13), the influence of water (15) and the uniaxial compressive strength (7) result in a RMR value of 70. Using this value, the constant  $s$  can then be calculated:

$$s = \exp(70-100)/9 = 0,035$$

The constant  $s = 0,035$  and the uniaxial compressive strength  $\sigma_c = 53,2$  MPa were used for the subsequent Hoek rock strength calculation. Finally, with these parameters, the rock strength  $\sigma_{1s}$  can be calculated:

$$\sigma_{1s} = \sqrt{0,035 * (53,2)^2} = 9,3 \text{ MPa}$$

The shear stress  $\tau$  [MPa] determined from the shear tests is plotted against the normal stress  $\sigma$  [MPa] in a plot. As a result, the angle of friction of the investigated discontinuities can be determined. The Figure 12 shows the shear and normal stresses of the two tested samples UV S 1 and UV S 2.

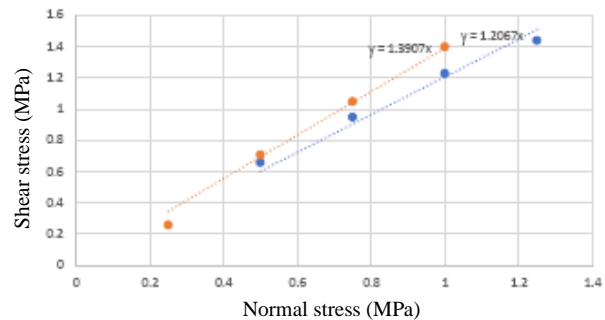


Figure 12. Results of the shear tests of the samples UV S1 (orange) and UV S2 (blue)

The friction angles  $\phi$  of the discontinuities of the respective samples were determined by means of the slope of the regression line. The friction angles are  $54^\circ$  for the sample UV S1 and  $50^\circ$  for the sample UV S2.

The resistance index  $I_{d2}$  determined by the slake durability test is 97,99% for the unweathered trachyte and 97,14% for the weathered samples. After the first cycle, the index  $I_{d1}$  is 98,57% or 97,78%, respectively.

### 3.2. Results of the discontinuity analysis

The pole points of the measured discontinuities of eleven measured scanlines are shown in the stereographic projection using the program Dips 7.0 [6] (see Figure 13).

The strike of the slope (260/89) is marked by the yellow colored line. The red circled areas represent the six distinct discontinuity systems distinguished scanline data.

Four main discontinuity systems (set 1 - 4) can be distinguished. Set 2 has the highest density of pole points. In addition, two other discontinuity systems can be seen in the stereographic projection (Set 5 and 6), which are weakly represented. Since these areas were also used to determine the failure criteria and further evaluation, these had to be combined into two sets.

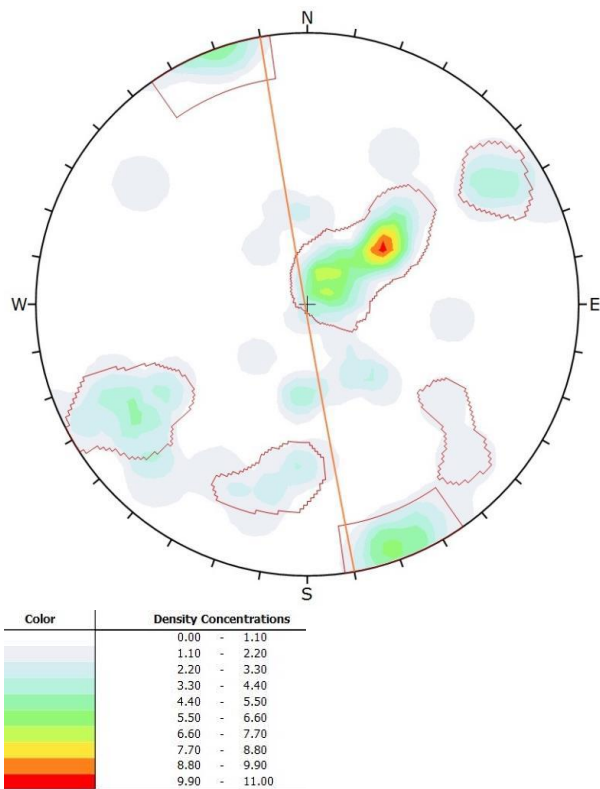


Figure 13. Stereographic projection of the discontinuities of the scanline measurements

The stereographic projection shows the pole points of the discontinuities, which were determined by means of the borehole television (see Figure 14).

The stereographic projection shows five different discontinuity systems. The highest density of pole points occurs in Set 4. In addition, set 1, which also has a large number of pole points.

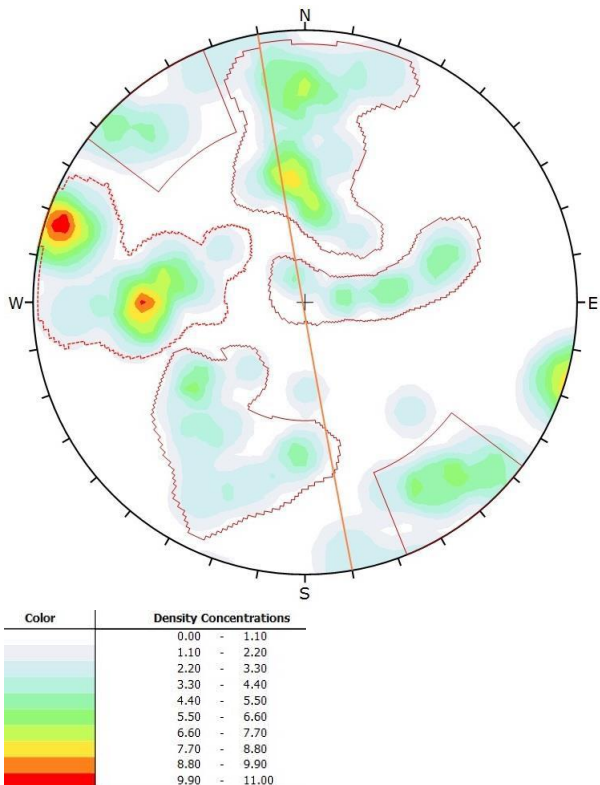


Figure 14. Stereographic projection of the discontinuities of the television measurements

The discontinuity system determined from the LIDAR data are plotted in the stereographic projection of Figure 15.

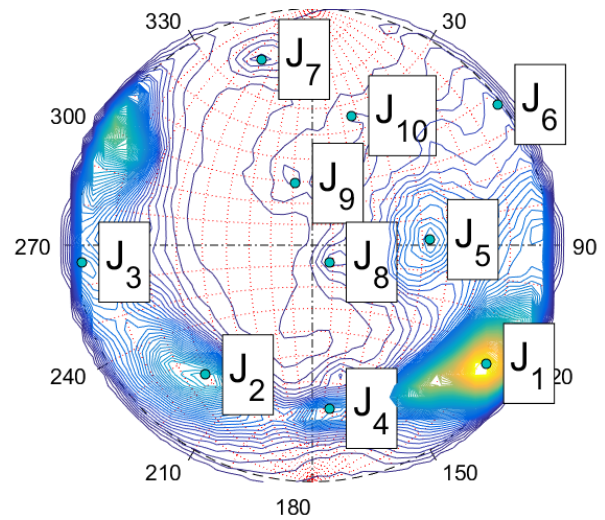


Figure 15. Stereographic projection of the discontinuities of the LIDAR measurements

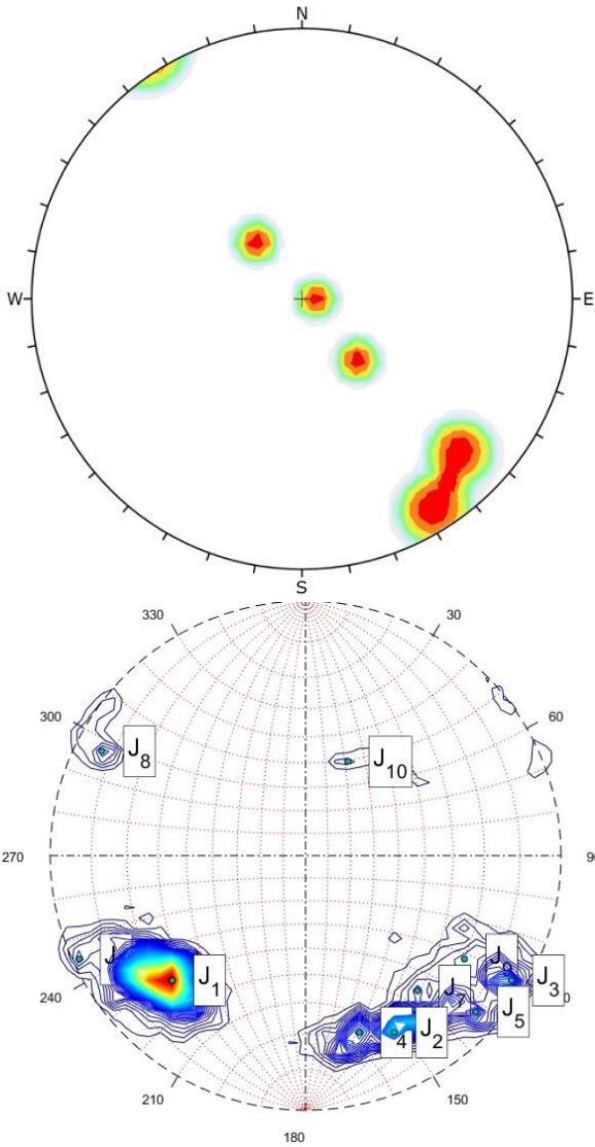
The LIDAR data were processed using the *Cloud Compare* program. The calculation of the discontinuity systems and representation of the stereographic projection were carried out by the program *Discontinuity Set Extractor*. Table 3 shows the 10 determined discontinuity sets. The set J1 with a share of 40% is most strongly represented. Other discontinuity systems that are strongly represented are formed by Set J3 (16%) and Set J2 (10%).

Table 3. Discontinuity sets and their orientations

Set	Dip direction [°]	Dip angle [°]	Proportion [%]
J1	304	83	40
J2	039	71	10
J3	085	89	16
J4	354	69	7,3
J5	267	53	8,7
J6	232	89	8,5
J7	164	78	2,1
J8	315	11	1,7
J9	164	30	1,1
J10	196	59	2,5

The Figure 16 shows the evaluation of scanline and the LIDAR measurements.

In the scanline data, the structural data are dominant with a orientation of about 320/80. Moreover, discontinuities with orientations of about 141/30, 318/34 and 272/6 can be recognized. In the LIDAR measurements the area J1 with values of about 046/71 is most frequently represented by 50%. Some discontinuities have a dip direction between 301° and 343°, while the dip angle varies between 70° and 86°.



**Figure 16.** Comparison of the evaluation of scanline no. 2 (top) and LIDAR (bottom) measurements

Another data comparison is shown in Figure 17. In scanline 6 six discontinuities have been measured whose orientations are 222/46, 060/59, 210/65, 229/25 and 345/88. The LIDAR measurements revealed dominant planes of discontinuity with orientations of 314/83 (J1), 290/86 (J2) and 102/87 (J3).

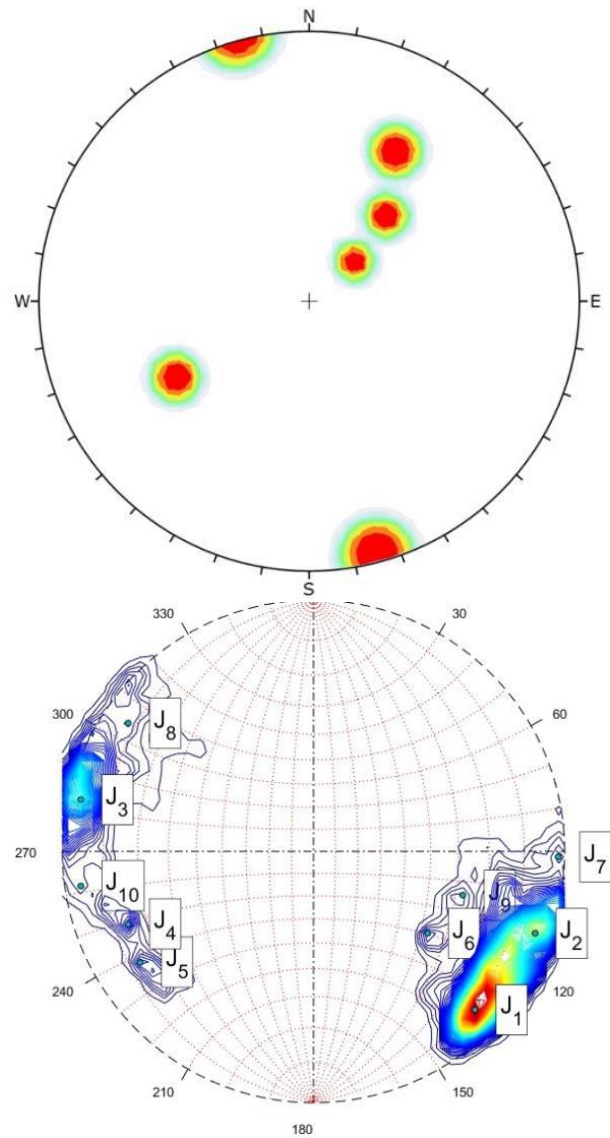


**Figure 17.** Comparison of the evaluation of scanline no. 6 (top) and LIDAR (bottom) measurements

### 3.3. Possibilities of slope failures

The kinematic failure possibilities of the investigated slope were determined using the program Dips 7.0 [6]. In the following chapters the identified failure possibilities are presented in stereographic projections.

#### 3.3.1. Toppling

Examination of the slope of the Drachenfels shows that the kinematic failure possibility consists of toppling. For the kinematic analysis, the laboratory-determined friction angle of 50° and a lateral limit of 30° were entered into the program. In addition, the slope parallel joints from set 4 of the television data were included in the calculation. The stereographic projection shows the range in which this failure mechanism is kinematically possible (see Figure 18).

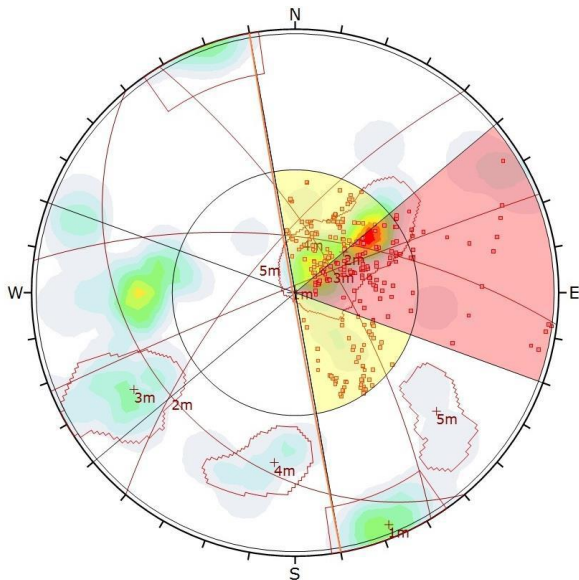


Figure 18. Toppling of the Drachenfels slope

In the stereographic projection, the area in which toppling kinematic is possible is colored red. The red dots are formed by the intersection points of the great circles of two dividing surface systems. In this range, the value of the friction angle  $\varphi_p$  is less than the fall angle  $\psi_p$ . Since some crossover points are in the red colored area, the occurrence of toppling is kinematically possible. The red-colored intersection points which lie outside the lateral boundary, do not form blocks in which the tilting is kinematically possible.

### 3.3.2. Wedge failure

The second failure mechanism found in the kinematic analysis is wedge failure. Also in this analysis the laboratory determined friction angle of  $50^\circ$  and a lateral limit of  $30^\circ$  were used. The analysis results are shown in the stereographic projection of Figure 19.

In the analysis, the slope parallel joints of set 4 of the television data were not included because they did not form any crossover points in the red colored area. Also in this case, the area in which wedge failure is kinematically possible is colored red. In this range, the fall angle of the blend linear is steeper than the friction angle. In addition, the crossover points of the major circles are in the area outside the slope. Since the intersection points of the large circles thus meet the kinematic conditions, the occurrence of wedge failure in this area is possible. For the further investigations of the failure possibilities these points were used.

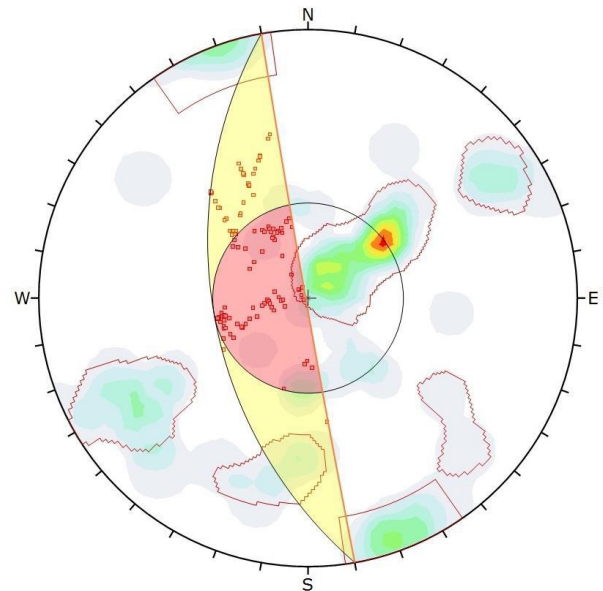


Figure 19. Wedge failure of the Drachenfels slope

## 3.4. Geometric analysis of failure possibilities

Based on the results of the kinematic analysis, possible failure modes were investigated geometrically. The following chapters describe examples of the modeling results that were performed with the RocTopple 1.0 [7] and Swedge 6.0 [8] programs.

### 3.4.1. Toppling

Flat dipping discontinuities (dip angle:  $23^\circ$ ) of Set 2 were defined as detaching discontinuities in the detailed analysis of the possible fall of boulders. Since no boulder height can be entered in this program, a value of the slope height a few meters was chosen that corresponds with the discontinuity spacing of Set 2. The width of the blocks is defined by the discontinuity spacing of the sets being examined. Here, the discontinuity systems are examined which have a relatively steep dip and have also formed intersection points in the kinematic analysis of the vulnerable zone. In the first two examples, Set 3 was investigated with a dip angle of  $71^\circ$  and a spacing of 3 m and 1,5 m. The results of this analysis are shown in the Figures 20 and 21.

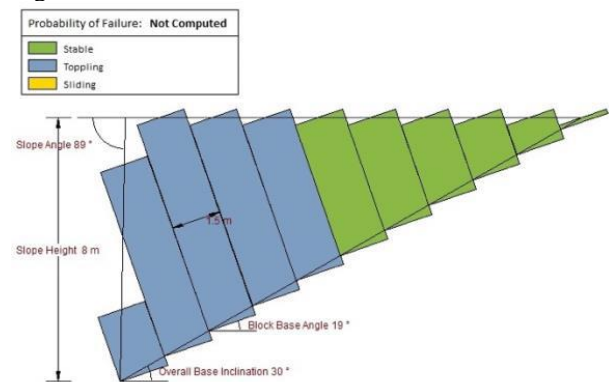


Figure 20. Toppling analysis of Set 3 – spacing 1,5 m

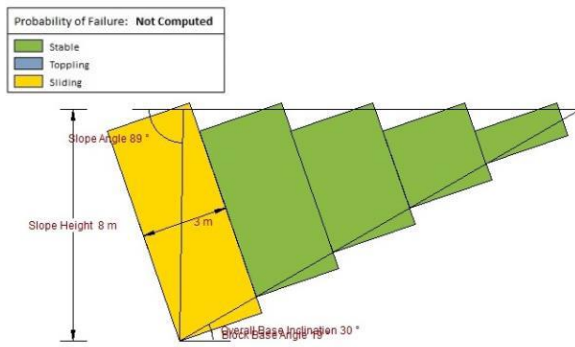


Figure 21. Toppling analysis of Set 3 – spacing 3 m

With a spacing of 1,5 m, half of the boulders are safe, with the other half toppling is possible. The spacing of 3 m shows that most of the blocks are stable. Landslides can only occur in the range of the first block.

In the following example, Set 4 was analysed with a dip angle of 66°, a spacing of 0,8 m and 1,5 m and a slope height of 5,2 m. The height of 5,2 m corresponds to the lowest possible value that could be entered for the slope height in the program. Since the discontinuities of the other sets are smaller, an attempt was made to choose the lowest possible value. The results of the study are shown in Figures 22 and 23.

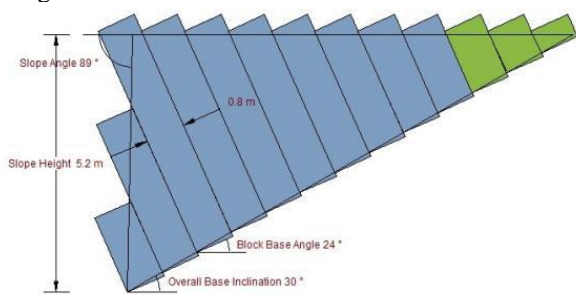


Figure 22. Toppling analysis of set 4 – spacing 0,8 m

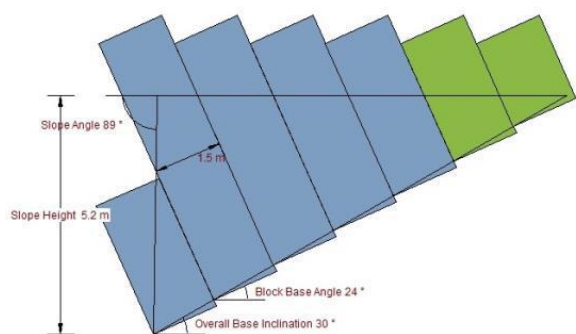


Figure 23. Toppling analysis of set 4 – spacing 1,2 m

With a spacing of 0,8 m, toppling is possible in the majority of the blocks (10 out of 13). If the spacing is increased to 1,5 m, toppling is still possible. In relation to the number of blocks, however, a larger area is stable.

### 3.4.2. Stabilization of unstable boulders

The stabilization of unstable boulders were also carried out using the program RocTopple 1.0 [7] by the introduction of rock anchors. The Figure 24 shows the anchorage of the unstable blocks of Set 3 with a spacing of 1,5 m.

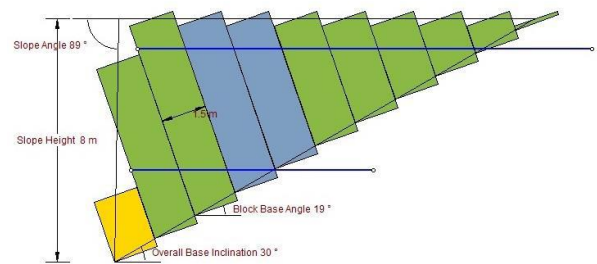


Figure 24. Stabilization of set 3

By installing two rock anchors, the first two larger blocks are secured. The lowest block can not fall, but there is the possibility of a slide.

### 3.4.3. Analysis of wedge failures

In the analysis of possible wedge failures, two discontinuity systems were combined, which form an intersection point in the stereographic projection in the endangered area (set 1, 3, 4, 5 and 6 of the scanline data). To check and construct a sliding wedge, several parameters were entered into the program. These consisted of the orientations and the lengths of the discontinuities, the friction angle of 50°, the rock density of 22 kN/m<sup>3</sup> and the geometry of the slope. Subsequently, a probabilistic analysis was performed with a sample number of 10000. The probability of failure of the sliding wedge results from the number of samples having a safety factor is less than 1. The results show the sliding wedges whose safety factor calculated by the software is less than 1. By comparing sets 1 (338/87) and set 6 (236/78) with discontinuity lengths of 10 m and 12 m, a sliding wedge was constructed with an average size of 22 m<sup>3</sup> (see Figure 25). The figure shows the sliding wedge from the front perspective.

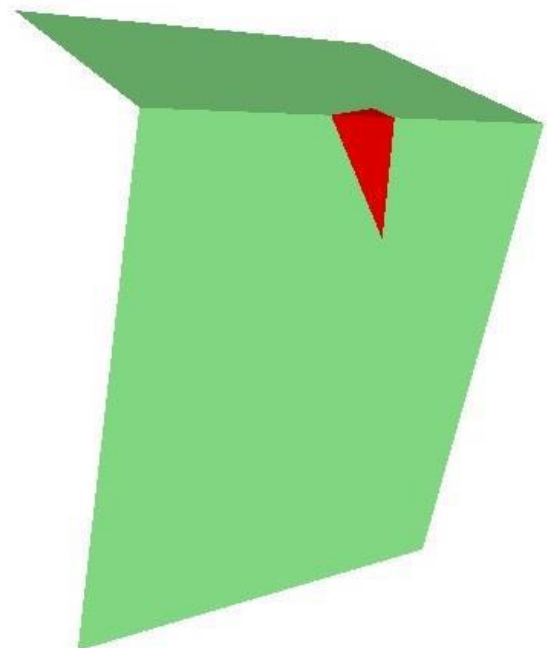


Figure 25. Sliding wedge constructed from set 1 and 6 with a volume of 22 m<sup>3</sup>

The probability of failure of the sliding wedge is 85% (85% < SF = 1). The average safety factor of the sliding

wedge is 0,52. Figure 26 shows that the probability of wedges failure is 85 %.

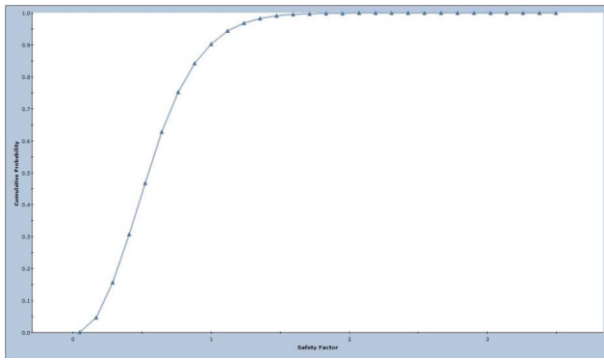


Figure 26. Failure probability of sliding wedges of sets 1 and 6

In order to check a possible change in the stability of the sliding wedges with a change in the friction angle of the discontinuities, the analysis was carried out again with a friction angle of 45°. The average safety factor drops to 0,45 with a probability of failure of about 90%.

Another sliding wedge construction, which has an average safety factor < 1, results from the comparison of Set 5 (308/75) and Set 6 (236/78). The discontinuity lengths are 8,2 m and 7,1 m. This results in a sliding wedge with an average volume of 20 m<sup>3</sup>. The failure probability of the wedge is 76%, while the average safety factor of the wedge is 0,82.

For this sliding wedge, the analysis was also repeated with a friction angle of 45°. This results in an average safety factor of 0,72 with a failure probability of 90%.

### 3.4.4. Stabilization of unstable sliding wedges

The stabilization of the sliding wedges which have a safety factor < 1 were made by installing rock anchors with the Swedge 6.0 [8] program.

To stabilize a sliding wedge formed by the discontinuities of Set 1 and Set 6, a minimum of 3,7 m long anchor with a capacity of 170 kN must be installed. The dip direction in which the anchor must be installed is 104° and the dip angle is 21° (see Figure 27).

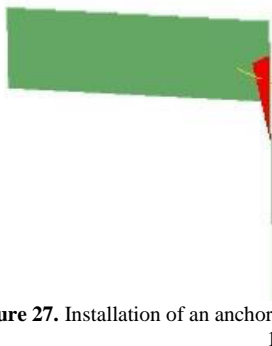


Figure 27. Installation of an anchor to stabilize sliding wedge No. 1

This stabilization measure raises the average safety factor to 1,56 and reduces the probability of failure to 11%.

The sliding wedge which is formed by the discontinuities of Set 5 and Set 6 must be stabilized by a minimum of 4,9 m long anchor with a capacity of 200 kN. For an optimal stabilization, the anchor has to be

installed horizontally with a dip direction of 80°. This stabilization measure increases the safety factor to a value of 2,04 and the failure probability of the slide wedges is 0%.

### 3.5. Risk assessment of rock falls

The final analysis includes the risk assessment of possible landslides at the slope of the Drachenfels. The analysis were carried out with the program RocFall 6.0. For every modeled rock fall, a number of 30 boulders were selected which fall from the slope at a horizontal speed of 1,5 m/s. The size of the boulders is 0,8 m<sup>3</sup>, i.e. edge length of 0,92 m. Moreover, the fall height of the boulders and the material lying at the foot of the slope were varied. A impact distinction was made between the accumulated debris (dyed green) and the already fallen trachyte boulders (light brown).

The first results show the course of a possible drop fall from the top impacting debris at the foot of the slope (gray). The result of this study is shown in the Figure 28.

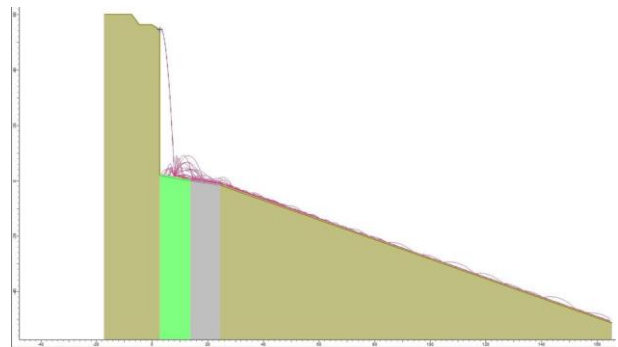


Figure 28. Rock fall from a height of 60 m impacting in debris

The modeling shows the flight curve and the further course of the boulders during a rock fall. The underlying debris is colored green in the Figure 28. The gray color indicates the foot path and the light brown color the trachyte.

The boulders bounce at a distance of about 8 m from the slope foot with a kinetic energy of about 55 kJ. The modeling shows that after the first impact, some boulders fall on the foot path (gray) at a height of approx. 8 m and roll down the slope. The boulders plunging towards the foot path have a kinetic energy of 70 kJ. It decreases to 24 kJ with a further locomotion. From initial 30 boulders, 19 boulders roll towards the valley. A small part of the boulders bounces off the debris towards the slope.

The Figure 29 shows the result of the rock fall that impact other boulders at the foot of the slope.

In this case, the boulders also bounce at a distance of 8 m from the slope. Differences can be seen in the kinetic energy and the rebound height of the boulders. The kinetic energy amounts to approx. 79 kJ after the impact of the boulders which are then hurled partly at a height of 10 m onto the foot path. The kinetic energy differs and rises to 100 kJ due to the further collapse of the boulders. Compared to the previous simulation, 25 out of 30 boulders fall down the entire slope. A small proportion of five boulders rebounds in the direction of the slope.

The simulation of a rock fall from a height of 40 m shows that parts of the boulders reach the foot path both

with underlying debris and underlain rock and the boulders continue to fall down the Drachenfels. At a rockfall height of about 18 m, the rock masses collide with construction rubble. Then only a few boulders roll in the direction of the foot path.

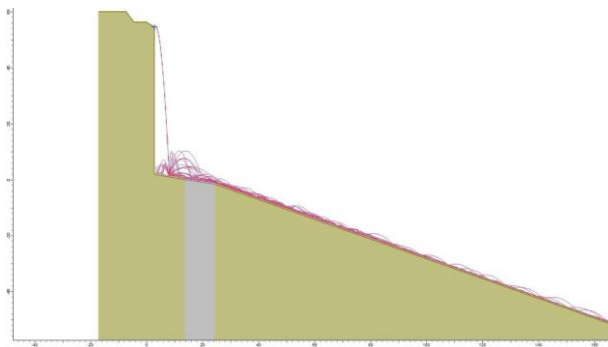


**Figure 29.** Rock fall from a height of 60 m impacting in trachyte boulders

In another analysis, a rockfall was simulated from about 10 m height (see Figure 30).

In this simulation, the boulders collide with the construction rubble lying below. A small part of the boulders roll in the direction of the foot path.

Most boulders remain in the immediate vicinity of the slope after the first impact. The kinetic energy after the first impact is 18 kJ and then decreases to 1,89 kJ. Four boulders move in the direction of the foot path and beyond with a kinetic energy of 7 kJ.

In a simulated rock fall with subjacent boulders, the kinetic impact energy is 25 kJ and then decreases to 5 kJ. One significant difference is the number of boulders that can fall further the foot path (16 out of 30 boulders).

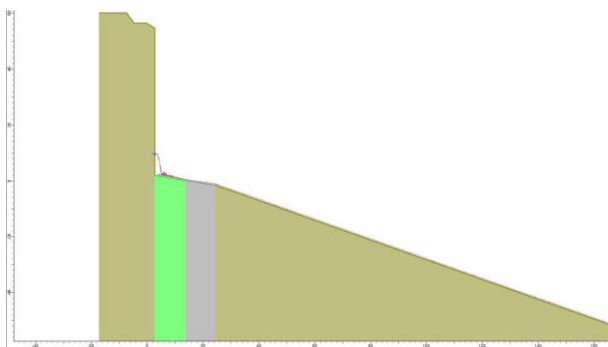


**Figure 30.** Rock fall from a height of 10 m impacting debris

## 4. Conclusions of the investigation

### 4.1. Rock mechanical properties

Results show that both the weathered and the unweathered trachyte have a high resistance to mechanical abrasion under the influence of water. Based on this and the results of the freeze-thaw tests, it can be concluded that the abrasion of the material and the destruction of the microstructure are primarily a consequence of the frost effect and the concomitant cryofracturing. The effect of water does not change the friction angle and other rock properties. Only by the freezing of the water the discontinuities and rock properties are influenced.

### 4.2. Structural geology

For the analysis of the slope stability, it can be concluded that above all the influence of frost and the high friction angle of the discontinuities are important factors. By cryofracturing the structure can be destroyed and thus lead to a decrease in cohesion. As a result, the cohesive forces are reduced and weaken thus the stability of the slope. The analysis of the friction angle shows that, due to its high value, it is very important for the stability of the slope. Due to the high friction angle, the probability of failure of wedges and toppling is significantly reduced. As a result, the stabilization measures at the Drachenfels comprise the closure of the open joints. The failure of the rock by a superposition of uniaxial compressive strength and rock strength could be excluded by the tests and analyses carried out.

It is noteworthy that the scanline data does not include two main orientations of discontinuities which are common in televue and LIDAR data. These are discontinuities that have a north-westerly direction and are almost vertical (dip angle 83°). These discontinuities are marked in the LIDAR data as set J1 but it is hardly represented in the televue data. In some areas, the slope orientation corresponds to this direction. It is the slope surface that corresponds to the final state of the old quarry wall. This surface represents a natural joint in which the rock was formerly quarried. These joints could hardly be measured with the scanline measurements (only two measured values, see Set 5). Since they run parallel to the slope and thus do not cut the tensioned measuring tape. The low occurrence of these discontinuities in the televue data is initially due to the fact that the three borings were not performed in the slopes where these fractures occur mainly. Another reason is that the borings run parallel to the strike of the discontinuities and therefore not cut them.

Other discontinuities which have a steep dip angle of almost 90°, is represented by Set 4 (televue) and Set J3 (LIDAR). In areas where the slope has a north-south strike these discontinuities run parallel to the slope and therefore can not be detected by the scanline method.

The last identified joint direction which is mainly represented by the televue measurements (set 1), but also by the LIDAR data (set J7) with a small proportion (2,1%). It dips to the south and represents the east-west trending main joint direction. The sets J8-J10 are identified by the LIDAR measurements as discontinuities but due to the low occurrence of these joints and the poor agreement with the manual measurements and televue data these discontinuities can be recognized as artifacts and not as the main joint direction. Based on the manual measurements, the televue and LIDAR data, seven main joint orientations have been identified by manual measurements from sets 1, 2, 3, 4 and 5 (partial) and by televue analyzes from sets 1 and 4.

The comparison of manual measurements and LIDAR measurements shows differences in the structural data in both stereographic projections. The reason for the differences is that in both cases the main joints in the LIDAR measurements are formed by the slope-parallel joints. A comparison of the manual measurements of the slope confirms the assumption that the set J1 in both

projections are joints represented by the slope wall. Apart from these values, further minor differences occur. Thus, e.g. the discontinuities which fall in a southwesterly direction, are not identified by the laser. Since the structural data in principle agree in many areas, this discrepancy may be due to the fact that it was difficult to select the exact area of the scanline when viewing the point cloud. However, when performing laser scanning, the data should be treated with caution, as it depends on the exact setting of the measuring device and good application knowledge. An inaccurate adjustment, the occurrence of e.g. an extremely rough or irregularly running discontinuity may lead to an identification of several discontinuities. This fact is reflected in Figure 16 where the stereographic projection of the laser data identifies six distinct joint sets that can normally be grouped into one set. In addition, ten discontinuity systems are identified on the basis of the laser data both in the overall evaluation and in individual areas of the slope. This number of discontinuity systems is not confirmed by comparison with manual measurements and television data. The erratic distribution of the discontinuities is also clear from the evaluation of the LIDAR data. When measuring and evaluating the data, care must be taken to ensure that the settings are correct and that the plausibility of individual partition systems is checked. For identification of erratically distributed fracture systems on a slope, it is therefore appropriate to perform manual measurements.

For the analysis of slope stability, it is important to identify the exact number of discontinuity systems as these are used to investigate the failure mechanisms. Therefore, it is important to make accurate measurements and compare different datasets. Too large a number of discontinuity systems can falsify the investigation and lead to a construction of wedges and boulders that do not exist in reality. The evaluations of the various measurements identified seven different discontinuity systems of the slope which are used for the analysis of slope stability.

When evaluating the discontinuity frequencies of the scanline and television data, it becomes clear that the discontinuity frequencies increase in the outer slope areas to the north and south. This effect is especially obvious with the television data, as the borehole televisions No. 4 to 9 were carried out below the retaining wall in the southern area of the slope, where the discontinuity frequency increases significantly. This fact is also evident when looking at the scanline data, as the traverses 10 and 11 were taken in the outer northern area of the slope and also because the discontinuity frequency shows higher values. It can therefore be concluded that in the areas farther away from the former volcanic pipe several discontinuities were formed by a faster cooling of the magma.

### 4.3. Failure mechanisms of the slope

The investigation of the Drachenfels shows that the occurrence of rock falls and wedge failures is kinematically possible. For an actual failure, geometric conditions such as the ratio of the width to the height of boulders must be fulfilled. A planar failure at the slope is

not possible due to the geometric conditions, e.g. the high friction angle of the discontinuities.

#### 4.3.1. Toppling

A detailed analysis of the failure possibilities using the RocTopple 1.0 software shows that the discontinuities of Set 3 (059/71) and Set 4 (007/66) form boulders with a risk of rock falling. In the analysis of the steeply dipping discontinuities of Set 3 to the northeast, it becomes clear that unstable blocks can only be formed with a smaller spacing (1,5 m in the example). However, this spacing is an estimated value, as the structural analysis of dips gave only a value of 3,08 m. As the discontinuities become larger, the ratio of the width to the height of the boulder and the stability increases. This fact prevents the boulders from falling. The first unstable boulder could be stabilized by a five-meter rock nail or anchor. The boulder behind it could be additionally stabilized by a twelve-meter-long anchor, which would have a much lower capacity. The other boulders behind can not fall, if the front boulders are stabilized by anchors.

Analysis of the north-facing discontinuities with a dip angle of  $66^\circ$  shows that most of the boulders are unstable if the spacing is smaller than 0,8 m. The first unstable boulder by installing a rock nail or anchor with a length of at least six meters. The nails or anchors have to be longer if the spacing is larger.

Overall, the steeply dipping discontinuities with a northern dip direction form unstable blocks on the investigated slope. The slope parallel joints which were included in the analysis from the television data do not form intersection lines with other joints and show no potential for toppling. The analysis of the discontinuities using the program RocTopple 1.0 [7] shows some inaccuracies with respect to toppling because the properties of only one discontinuity can be entered in the program. The spacing of the second boulder forming discontinuity which were entered into the program as the slope height did not correspond to the actual spacing. For these reasons, the estimation of the instability of the boulders is only a rough estimation.

When looking at the number of unstable boulders, it seems realistic that many of these rock masses have already fallen over time.

#### 4.3.2. Sliding wedges

The analysis of the sliding wedges allows a more precise statement, as more parameters are used in the program Swedge. Sliding wedges are formed with a safety factor below 1 by intersecting joints that dip steeply to the north-west and joints that dip steeply to the south-west. These wedges tend to fail. The wedge size of  $22 \text{ m}^3$  seems realistic, although boulders with a size of  $50 \text{ m}^3$  fell in the past. Due to smaller joint lengths, boulders are expected to have a smaller volume.

Another sliding wedge with a safety factor less than 1, is a result of the intersection joints of Set 5 (308/75) that are parallel to the slope and joints that dip steeply towards the south-west. Also, this sliding wedge size of  $20 \text{ m}^3$  with a length of 8,2 m and 7,1 m respectively seems to

be realistic. For both sliding wedges, it is necessary to install anchors with a significantly higher capacity (170 kN and 200 kN) than for the previously discussed boulders. It is important to notice that the safety factor decreases with the decrease of the friction angle. It can be assumed that properties such as the friction angle of the discontinuities decrease over time and the safety factor as well.

#### 4.4. Risk assessment of possible rock falls

The simulation of the slope failures shows that especially rock falls from the top of the slope represent a considerable risk potential. The fallen boulders bounce off the debris or boulders at the foot of the slope with a kinetic energy of approx. 70 kJ after the first impact. This is a direct threat to users of the foot path along the slope. Another risk consists in the potential rock falls endangering areas of the city of Königswinter and the railway near the Rhine river. In the modeling it became clear that there is a danger from boulders with a weight of 1000 kg and a size of about 1 m<sup>3</sup>. However, it became apparent from the failure analysis that even larger boulders and wedges with sizes of up to 20 m<sup>3</sup> can fall. Accordingly, the kinetic energy and the risk potential is much higher.

#### 5. Measures of rock stabilization

Within the framework of the rock stabilization measure at the Drachenfels more than 200 rock anchors, nails and tendons were installed as well as about 1500 m<sup>2</sup> of rock were shotcreted in order to prevent the rock from sliding and falling (see Figure 31).

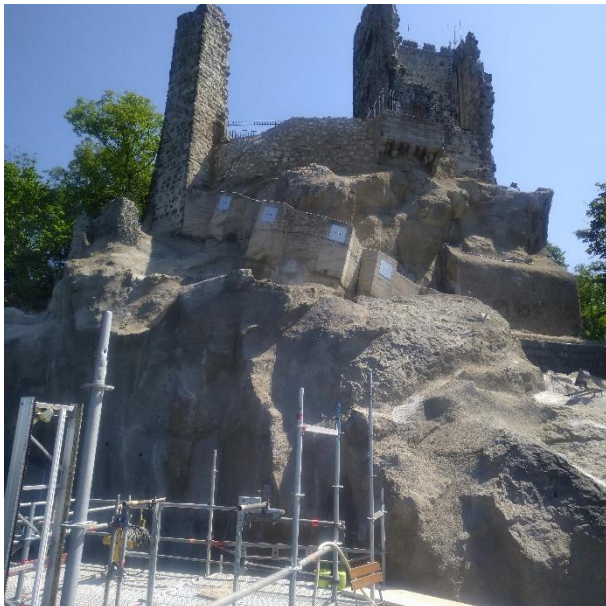


Figure 31. Stabilization of the Drachenfels by anchors, nails and shotcrete

Another important aspect was the closure of about 400 m of larger and open joints with a special mortar to minimize the penetration of precipitation into the rock mass. Tests have shown that the penetration of water in conjunction with the frost can have a significant impact on the mechanical properties (including friction angle) of

the discontinuities. The friction angle of the discontinuities is very high (50°). Therefore, it is important for the stability of the slope that this value of the friction angle will not be exceeded. The closing of the joints prevents the entry of water and thus the influence of frost on the rock mass. It is particularly important to close the joints in the upper areas of the slope.

An approximately 150 m<sup>2</sup> rock area was stabilized by a cap of a back-anchored spiral rope net made from high-tensile wire that is able to secure loose, blocky rocks, rock spurs, overhangs or unstable rock formations with highly irregular surface structures. This system utilizes a flexible nail grid and boundary ropes together with the spiral rope net. (see Figure 32). The rock outcrop that had to be stabilized and secured this way has a total height of about 7,7 m, a length of about 2,1 m and a width of about 1,2 m. This results in a volume of approximately 19,4 m<sup>3</sup>. A good third, i.e 7 m<sup>3</sup> to 8 m<sup>3</sup>, had to be secured with a net of about 200 m<sup>2</sup>. The net had to carry a weight of about 15 t to 18 t.

In addition, the coarse-meshed net was combined with a finer-meshed secondary net in order to prevent the falling of smaller rocks that fit through the coarse meshes.

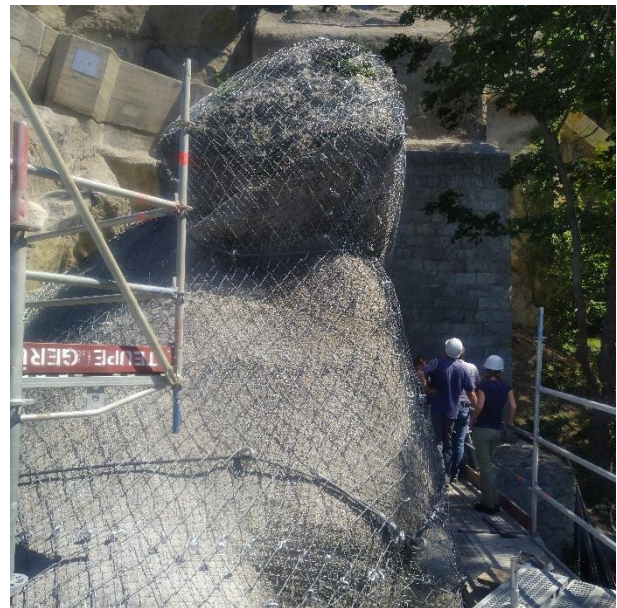


Figure 32. Rock secured and stabilized by a spiral net

#### References

- [1] EN 12371, Natural stone test methods - Determination of frost resistance, 2010-07
- [2] Priest, S.D. & Hudson J.A., 1981. Estimation of Discontinuity Spacing and Trace Length Using Scanline. *International Journal of Rock Mechanics and Mining Sciences and Geomechanics Abstracts*, 18, 183
- [3] Riquelme, A.J., Abellán, A., Tomás, R., Jaboyedoff, M., 2014. A new approach for semiautomatic rock mass joints recognition from 3D point clouds. *Comput. Geosci.* 68, 38–52. <http://dx.doi.org/10.1016/j.cageo.2014.03.014> URL: <http://www.sciencedirect.com/science/article/pii/S0098300414000740>.
- [4] Riquelme, A.J., Abellán, A., Tomás, R., 2015. Discontinuity spacing analysis in rock masses using 3D point clouds. *Eng Geol.* 195: 185–19 <http://dx.doi.org/10.1016/j.enggeo.2015.06.009>, URL (<http://www.sciencedirect.com/science/article/pii/S0013795215002045>).

- [5] Wunderlich, H.-G., 1968. Einführung in die Geologie. Band 2: Endogene Dynamik. - BI Hochschultaschenbücher, Band 341.

## **Software**

- [6] Dips 7.0., Rocscience Inc., 54 Saint Patrick St., Toronto, ON M5T 1V1, Canada, [www.rocscience.com](http://www.rocscience.com)
- [7] RocTopple 1.0, Rocscience Inc., 54 Saint Patrick St., Toronto, ON M5T 1V1, Canada, [www.rocscience.com](http://www.rocscience.com)
- [8] Swedge 6.0, Rocscience Inc., 54 Saint Patrick St., Toronto, ON M5T 1V1, Canada, [www.rocscience.com](http://www.rocscience.com)
- [9] CloudCompare, [www.cloudcompare.org/](http://www.cloudcompare.org/)
- [10] FaroScene, FARO Europe GmbH & Co. KG, Lingwiesenstr. 11/2, 70825 Korntal-Münchingen, Germany, [www.faro.com](http://www.faro.com)